Article:
Zhang, J.-L., Sun, E.-C., Zhuang, P.-Z. et al. (2 more authors) (2024) Elastoplastic solution for cylindrical cavity contraction in unsaturated soils. Géotechnique Letters, 14 (1). pp. 1-7. ISSN: 2045-2543

https://doi.org/10.1680/jgele.23.00080

Elastoplastic solution for cylindrical cavity contraction in unsaturated soils under constant suction conditions

Mr Jia-Liang **Zhang**[1], Postgraduate Student Email: zhangjialiang@mail.sdu.edu.cn;

Mr En-Ci **Sun**[1], Postgraduate Student Email: sunenci@mail.sdu.edu.cn;

Prof Pei-Zhi **Zhuang**[1] Email: zhuangpeizhi@sdu.edu.cn;

Prof Hai-Sui **Yu**[2]**,** FREng E-mail: H.Yu@leeds.ac.uk;

Mr He **Yang**[2], PhD Candidate E-mail: yanghesdu@mail.sdu.edu.cn;

[1]School of Qilu Transportation, Shandong University, Jinan, 250002, China

[2]School of Civil Engineering, University of Leeds, Leeds, LS2 9JT, UK

Abstract: This letter develops an elastoplastic solution for cylindrical cavity contraction in unsaturated soils under constant suction conditions. The elastoplastic cavity contraction problem is formulated into a set of first-order ordinary differential equations (ODEs) by introducing a new auxiliary variable, which is solved as an initial value problem. The new solution is validated by comparison with numerical simulation results. Finally, parametric studies show that, as soil suction increases, the internal support pressure decreases faster with cavity contraction, the unloading-induced plastic zone becomes narrower, and the changes in effective stresses are smaller for a given tunnel convergence.

Keywords: Ground response curve; unsaturated soil; cavity contraction; tunnels & tunnelling; plasticity; stress analysis

Introduction

The relationship between support pressure and tunnel convergence (i.e. ground response curve, GRC) is vital for tunnel design with the convergence-confinement method (Brown et al. 1983; Park et al. 2008). Very often GRC is predicted by the elastoplastic cavity contraction theory that studies the development of stresses and displacement around a contracting cylindrical cavity (Yu 2000). For example, a number of cavity contraction solutions were available for soils and rocks with various constitutive models, such as the Mohr-Coulomb model (Yu and Rowe 1999; Carranza-Torres 2003; Vrakas and Anagnostou 2014), Hoek-Brown failure criteria (Brown et al. 1983; Zareifard 2020; Guan et al. 2022; Cai et al. 2023), strain hardening/softening Drucker-Prager model (Chen et al. 2012; Chen and Abousleiman 2017), and critical state (Cam Clay) models (Yu and Rowe 1999; Chen and Abousleiman 2016; Mo and Yu 2017; Zhuang et al. 2020). Also, some cavity contraction solutions were developed to investigate the influence of soil anisotropy (Chen H et al. 2022), ground surface (Zhuang et al. 2022), non-hydrostatic in-situ stress field (Ma et al. 2023), seepage pressure (Sun et al. 2023; Zhao et al. 2023), and plane stress conditions (Yang et al. 2022) on the characteristics of GRCs.

Soils in the region affected by groundwater and rainfall are normally in an unsaturated state. GRC for tunnelling in unsaturated soils ought to be affected by suction and degree of saturation. However, to the best knowledge of the authors, cavity contraction solutions for unsaturated soils have not been reported yet. To fill the gap, this letter provides an elastoplastic solution for cavity contraction in unsaturated soils under constant suction conditions. The work is an extension of Chen H et al. (2020) to the cavity contraction scenario, and a modified auxiliary variable is introduced to transform the governing equations into a set of first-order ordinary differential equations (ODEs). Finally, a parametric study is conducted to highlight the influence of suction on GRC, stress paths, and stress distributions.

Problem Definition and Assumptions

This letter considers the contraction of a cylindrical cavity with an initial radius a_0 and infinite length in the axial direction, as shown in Figure 1. The soil around the cavity is of infinite radial extent and is modelled by an elastoplastic unsaturated model. Prior to unloading (i.e. initial state), total horizontal and vertical stresses (σ_{h0}, σ_{v0}) act throughout the soil, and the initial suction and degree of saturation are s_0 and S_{r0}, respectively. Note that the initial stress state is shown in a general form in order to extend the potential applications of the solution, and it can be assumed that $\sigma_{h0}=\sigma_{v0}$ for tunnelling and $\sigma_{h0}\neq\sigma_{v0}$ for other

excavation problems such as wellbore drilling (Chen and Abousleiman 2016; Chen and Abousleiman 2017; Chen S et al. 2022). Then the internal support pressure gradually reduces from σ_{h0} to σ_a, while the radius of the inner cavity reduces from a_0 to the current radius a. In the contraction process, an unloading-induced plastic zone forms in the region of $a \le r \le \rho$, where ρ is the current radius of the elastoplastic boundary. For convenience the present cavity contraction problem is accounted for by the cylindrical polar coordinates (r, θ, z) with the origin at the cavity centre.

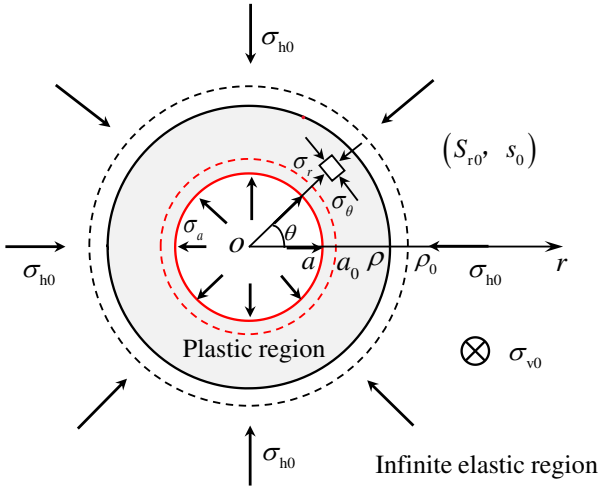

Figure 1 Schematic of the cylindrical cavity contraction problem

The following commonly used assumptions are adopted for the theoretical analysis of cavity contraction in homogenous and isotropic soils, including (Brown et al. 1983; Yu 2000; Xu and Xia 2021):

(a) The plane strain assumption is satisfied for a long tunnel.

(b) The stresses and geometry boundary conditions are axisymmetric.

(c) The unloading process is sufficiently slow so that the dynamic effect can be neglected.

Taking compressive stresses/strains as positive, the equilibrium equation and boundary conditions for the axisymmetric problem can be expressed as

$$\frac{\mathrm{d}\sigma_r}{\mathrm{d}r} + \frac{\sigma_r - \sigma_\theta}{r} = 0 \tag{1}$$

$$\sigma_r\big|_{r=a} = \sigma_a \tag{2}$$

$$\sigma_r\big|_{r=\infty} = \sigma_{h0} \tag{3}$$

where σ_r and σ_θ denote the total radial and circumferential stresses, respectively; $\mathrm{d}(\bullet)$ denotes the

spatial differential of $(\bullet)$ for a given time (i.e. Eulerian description); r denotes the current radial position of a soil particle (i.e. material point).

Constitutive modelling of unsaturated soils

The unsaturated critical state model (UCSM) of Sun et al. (2007) is adopted for constitutive modelling of unsaturated soils, which is briefly introduced as follows. In UCSM the effective stress (i.e. average soil skeleton stress) and suction are selected as two stress state variables, defined as

$$\sigma'_{ij} = \sigma_{ij} - u_{\mathrm{a}}\delta_{ij} + S_{\mathrm{r}}s\delta_{ij} \tag{4}$$

$$s = u_{\mathrm{a}} - u_{\mathrm{w}} \tag{5}$$

where σ'_{ij}=effective stress tensor; σ_{ij}=total stress tensor; δ_{ij}=Kronecker's delta; S_{r}=degree of saturation; s=suction; u_{a}=pore air pressure (is assumed to equal the atmospheric pressure); u_{w}=pore water pressure.

In the $p'-q$ plane USCM shares the same yield surface shape with the modified Cam Clay model (MCC) as shown in Eq. (6) and Figure 2:

$$f = \left(\eta/M\right)^2 - \left[p'_{\mathrm{y}}(s)/p' - 1\right] = 0 \tag{6}$$

$$p'_{\mathrm{y}}(s) = p'_{\mathrm{n}}\left(\frac{p'_{\mathrm{y}}(0)}{p'_{\mathrm{n}}}\right)^{\frac{\lambda(0)-\kappa}{\lambda(s)-\kappa}} \tag{7}$$

$$\lambda(s) = \lambda(0)\left[(1-b)e^{-cs} + b\right] \tag{8}$$

where f denotes the yield function; $\eta = q/p'$ is the stress ratio; $p' = \sigma'_{ii}/3$ denotes the mean effective stress; $q = \sqrt{3\left(\sigma'_{ij} - p'\delta_{ij}\right)\left(\sigma'_{ij} - p'\delta_{ij}\right)/2}$ is the deviatoric stress; M denotes the slope of the critical state line (CSL) in the $p'-q$ plane; $p'_{\mathrm{y}}(s)$ is the isotropic yield stress at a suction of s; p'_{n} is a reference stress; $\lambda(s)$ and $\lambda(0)$ are the slopes of the normal compression line in the $v-\ln p'$ plane at suctions of s and 0, respectively; κ is the slope of the swelling line in the $v-\ln p'$ plane (independent on suction); $p'_{\mathrm{y}}(0)$ is the isotropic consolidation pressure at a suction of 0 (i.e. saturated soils); b and c are two material parameters for unsaturated soils (Alonso et al. 1990).

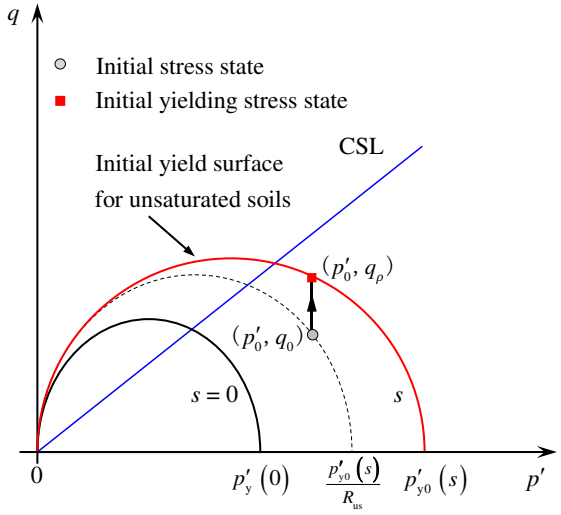

Figure 2 Yield surface in the $p'-q$ plane.

An associate flow rule and the volumetric hardening law are used in USCM, and the plastic volumetric stain $\varepsilon_v^{\mathrm{p}}$ satisfies:

$$\mathrm{D}\varepsilon_v^{\mathrm{p}} = \frac{\lambda(0)-\kappa}{v}\frac{\mathrm{D}p_{\mathrm{y}}'(0)}{p_{\mathrm{y}}'(0)} \tag{9}$$

where $\mathrm{D}(\bullet)$ denotes the material time differential of $(\bullet)$ for a given soil particle (i.e. Lagrangian description).

Under constant suction conditions, the soil water retention curve in Sun et al. (2007) can be simplified as

$$\mathrm{D}S_{\mathrm{r}} = -\lambda_{\mathrm{se}}\mathrm{D}v \tag{10}$$

where v =specific volume of unsaturated soils; λ_{se} =slope of the $S_{\mathrm{r}}-v$ curve at a constant suction.

Elastoplastic Solution

Solution in the elastic region

In the elastic region ($r>\rho$) the stress-strain relationship is assumed to obey Hooke's law and small strain definitions (Yu 2000; Chen H et al. 2020):

$$\begin{bmatrix}\mathrm{D}\varepsilon_r^{\mathrm{e}}\\ \mathrm{D}\varepsilon_\theta^{\mathrm{e}}\\ \mathrm{D}\varepsilon_z^{e}\end{bmatrix} = -\begin{bmatrix}\mathrm{d}(\mathrm{D}u)/\mathrm{d}r\\ \mathrm{D}u/r\\ 0\end{bmatrix} = \frac{1}{E}\begin{bmatrix}1 & -\mu & -\mu\\ -\mu & 1 & -\mu\\ -\mu & -\mu & 1\end{bmatrix}\begin{bmatrix}\mathrm{D}\sigma_r'\\ \mathrm{D}\sigma_\theta'\\ \mathrm{D}\sigma_z'\end{bmatrix} \tag{11}$$

where $\varepsilon_r^{\mathrm{e}}$, $\varepsilon_\theta^{\mathrm{e}}$ and $\varepsilon_z^{\mathrm{e}}$ denote the elastic radial, circumferential, and vertical strains, respectively; σ_r', σ_θ',

and σ_z' denote the radial, circumferential, and vertical effective stresses, respectively; $u = r - r_0$ represents the radial displacement of a soil particle whose initial radial position is r_0; E and μ are the elastic modulus and Poisson's ratio of soils, and E is expressed as

$$E = \frac{3(1-2\mu)vp'}{\kappa} \tag{12}$$

Combining Eqs. (1), (3), (4) and (11), the solution for stresses, displacement, volume change, and saturation degree in the elastic zone can be obtained following Yu (2000) and Chen H et al. (2020):

$$\sigma_r' = \sigma_{\mathrm{h0}}' + \left(\sigma_{r\rho}' - \sigma_{\mathrm{h0}}'\right)(\rho/r)^2 \tag{13}$$

$$\sigma_\theta' = \sigma_{\mathrm{h0}}' - \left(\sigma_{r\rho}' - \sigma_{\mathrm{h0}}'\right)(\rho/r)^2 \tag{14}$$

$$\sigma_z' = \sigma_{\mathrm{v0}}' \tag{15}$$

$$p' = p_0' = \frac{\sigma_{\mathrm{v0}}' + 2\sigma_{\mathrm{h0}}'}{3} \tag{16}$$

$$\frac{u}{r} = \frac{(1+\mu)}{E}\left(\sigma_{r\rho}' - \sigma_{\mathrm{h0}}'\right)(\rho/r)^2 \tag{17}$$

$$v = v_0 \tag{18}$$

$$S_{\mathrm{r}} = S_{\mathrm{r0}} \tag{19}$$

where σ_{h0}' and σ_{v0}' are the initial horizontal and vertical effective stress; p_0' and v_0 are the initial mean effective stress and initial specific volume; $\sigma_{r\rho}'$ denotes the effective radial stress in the elastoplastic boundary and can be determined by substituting Eqs. (13)-(17) into the yield function (6) (Chen and Abousleiman 2013; Chen H et al. 2020), as

$$\sigma_{r\rho}' = \sigma_{\mathrm{h0}}' - \sqrt{\left[q_\rho^2 - \left(\sigma_{\mathrm{h0}}' - \sigma_{\mathrm{v0}}'\right)^2\right]/3} \tag{20}$$

$$q_\rho = Mp_0'\sqrt{p_{\mathrm{y0}}'(s) - 1} \tag{21}$$

$$p_{\mathrm{y0}}'(s) = R_{\mathrm{us}}p_0'\left[1 + \left(q_0/Mp_0'\right)^2\right] \tag{22}$$

in which q_ρ denotes the deviatoric stress at $r = \rho$ and q_0 is the initial deviatoric stress; p_{y0}' is the initial isotropic pre-consolidation stress and R_{us} represents the initial overconsolidation ratio of unsaturated soils,

(see Fig. 2). Now the information at the elastoplastic boundary can be calculated by the elastic solution (Eqs. (13)-(22)), which provides initial values for solving the governing ODEs in the plastic region.

Solution in the plastic region

Following Sun et al. (2007) and Chen H et al. (2020), the incremental stress-strain relationship for unsaturated elastoplastic soils can be expressed as

$$\begin{bmatrix} \mathrm{D}\varepsilon_\theta \\ \mathrm{D}\varepsilon_z \\ \mathrm{D}\varepsilon_v \end{bmatrix} = \begin{bmatrix} B_{r\theta} & B_{\theta\theta} & B_{z\theta} \\ B_{rz} & B_{\theta z} & B_{zz} \\ B_{rp} & B_{\theta p} & B_{zp} \end{bmatrix} \begin{bmatrix} \mathrm{D}\sigma'_r \\ \mathrm{D}\sigma'_\theta \\ \mathrm{D}\sigma'_z \end{bmatrix} \tag{23}$$

where

$$B_{r\theta} = -\frac{\mu}{E} + \frac{A_r A_\theta}{K_\mathrm{p}} \tag{24}$$

$$B_{z\theta} = -\frac{\mu}{E} + \frac{A_z A_\theta}{K_\mathrm{p}} \tag{25}$$

$$B_{rz} = -\frac{\mu}{E} + \frac{A_r A_z}{K_\mathrm{p}} \tag{26}$$

$$B_{\theta z} = -\frac{\mu}{E} + \frac{A_\theta A_z}{K_\mathrm{p}} \tag{27}$$

$$B_{\theta\theta} = \frac{1}{E} + \frac{A_\theta A_\theta}{K_\mathrm{p}} \tag{28}$$

$$B_{zz} = \frac{1}{E} + \frac{A_z A_z}{K_\mathrm{p}} \tag{29}$$

$$B_{kp} = \frac{\kappa}{3vp'} + \frac{A_k A_\mathrm{p}}{K_\mathrm{p}} \quad (k = r,\theta,z) \tag{30}$$

$$A_k = \frac{\partial f}{\partial \sigma'_k} = \frac{M^2 - \eta^2}{3M^2 p'} + \frac{3(\sigma'_k - p')}{M^2 p'^2} \qquad (k = \theta, z) \tag{31}$$

$$A_p = \frac{\partial f}{\partial p'} = \frac{M^2 - \eta^2}{M^2 p'} \tag{32}$$

$$K_\mathrm{p} = \frac{v p'_y(0)}{\lambda(s) - \kappa} \frac{M^2 - \eta^2}{M^2 p'^2} \left(\frac{p'_y(0)}{p'_\mathrm{n}} \right)^{\frac{\lambda(0) - \lambda(s)}{\lambda(s) - \kappa}} \tag{33}$$

Note that the constitutive equation (23) is shown in the Lagrangian description while the equilibrium equation

(1) is in the Eulerian description. Following the pioneering work of Chen and Abousleiman (2013), Eq. (1) will be transformed into the expression of Lagrangian description by introducing a new auxiliary variable as follows.

The large deformation in the plastic region can be described by logarithmic strain definitions (Yu and Houlsby 1991; Yu 2000; Chen H et al. 2020), as

$$\varepsilon_r = -\ln\left(\mathrm{d}r/\mathrm{d}r_0\right) \tag{34}$$

$$\varepsilon_\theta = -\ln\left(r/r_0\right) \tag{35}$$

$$\varepsilon_{\mathrm{v}} = -\ln\left(v/v_0\right) = \varepsilon_{\mathrm{r}} + \varepsilon_\theta \tag{36}$$

Combination of Eqs. (34)-(36) leads to the compatibility equation related to r and v:

$$\frac{r_0\mathrm{d}r_0}{v_0} = \frac{r\mathrm{d}r}{v} \tag{37}$$

The cavity contraction process for the present problem is actually in a self-similar manner that all soil particles share the same stress and deformation paths (Chen and Abousleiman 2013; Chen and Abousleiman 2016). Hence, stresses/strains in the Eulerian description can be transformed into those in the Lagrangian description by auxiliary variables (e.g. $(r-r_0)/r$ and r_0/r) (Chen and Abousleiman 2013; Su 2021). In this letter $\ln\left(r/r_0\right)$ is involved as a new auxiliary variable, which can further simplify the derivation than former auxiliary variables. The incremental forms of $\ln\left(r/r_0\right)$ in terms of Lagrangian and Eulerian descriptions equal each other owing to the self-similar characteristic (i.e. $\mathrm{d}\left[\ln\left(r/r_0\right)\right] = \mathrm{D}\left[\ln\left(r/r_0\right)\right]$), thereby giving

$$\frac{\mathrm{D}r}{r} = \frac{\mathrm{d}r}{r} - \frac{\mathrm{d}r_0}{r_0} \tag{38}$$

Combining Eqs. (37) and (38), we can get

$$\frac{\mathrm{d}r}{r} = \frac{1}{1-\left(r/r_0\right)^2\left(v_0/v\right)}\frac{\mathrm{D}r}{r} \tag{39}$$

Then the equilibrium equation (1) can be rewritten in the Lagrangian description by substituting Eqs. (4), (10), and (39) into Eq. (1), as

$$\mathrm{D}\sigma_r' + \lambda_{\mathrm{se}}s_0\mathrm{D}v = \left(\sigma_\theta' - \sigma_r'\right)\left(\frac{r_0^2 v}{r_0^2 v - r^2 v_0}\right)\frac{\mathrm{D}r}{r} \tag{40}$$

Later, the ODEs for the elastoplastic cavity contraction process can be derived by combining Eqs. (23), (35), (36), and (40), as

$$\begin{bmatrix} 1 & 0 & 0 & \lambda_{se}s_0 \\ B_{r\theta} & B_{\theta\theta} & B_{z\theta} & 0 \\ B_{rz} & B_{\theta z} & B_{zz} & 0 \\ B_{rp} & B_{\theta p} & B_{zp} & 1/v \end{bmatrix} \begin{bmatrix} \mathrm{D}\sigma_r' \\ \mathrm{D}\sigma_\theta' \\ \mathrm{D}\sigma_z' \\ \mathrm{D}v \end{bmatrix} = \frac{\mathrm{D}r}{r} \begin{bmatrix} \dfrac{\sigma_\theta' - \sigma_r'}{1-(r/r_0)^2(v_0/v)} \\ -1 \\ 0 \\ 0 \end{bmatrix} \tag{41}$$

The ODEs can be readily solved with the initial values provided by the elastic solution at the elastoplastic boundary.

Finally, the radius in Eq. (41) should be seen in the form of Lagrangian description. In order to investigate field distributions, it is necessary to integrate Eq. (40) to obtain the equivalent radius in the Eulerian description (Chen and Abousleiman 2013; Chen H et al. 2022):

$$\ln\frac{r}{a} = \int_a^r \frac{1}{1-(r/r_0)^2(v_0/v)} \frac{\mathrm{D}r}{r} \tag{42}$$

Results and discussion

Based on the similarity between cavity contraction and tunnel convergence (Brown et al. 1983; Mair and Taylor 1993; Yu 2000), the influence of soil suction on GRCs, stress paths, and stress distributions is investigated using the developed cavity contraction solution with input parameters in Table 1 (Chen H et al. 2020; Chen S et al. 2020).

At first, finite element analyses (FEM) for cavity contraction in the dry soil (i.e. s_0=0) are conducted by ABAQUS 2020 following the numerical model of Yang et al. (2022), which can verify the accuracy of the proposed solution (e.g. Figure 3 and Figure 5).

Table 1 Input parameters for parametric study

σ_{h0}': kPa	σ_{v0}': kPa	p_0'	K_0	S_{r0}	p_{y0}': kPa	v_0	R_{us}
100	160	120	0.625	0.6	140.8	2.09	1
100	160	120	0.625	0.6	168.96	2.06	1.2
130	100	120	1.3	0.6	375.6	1.97	3

$M=1.2$, $b=0.65$, $c=0.125$, $\lambda(0)=0.15$, $\lambda_{se}=0.21$, $\kappa=0.03$, $\mu=0.3$, p_n'=10kPa

Figure 3 shows the influence of suction on the normalised GRCs with different overconsolidation ratios.

For a given R_{us}, it can be found that suction increase imposes an important impact on GRCs, which makes the normalised internal pressure decrease faster with tunnel convergence (i.e. $1-a/a_0$). Moreover, GRC is much steeper for a larger R_{us} because of the hardening effect of preconsolidation, and this is consistent with the observation in Chen and Abousleiman (2016) for dry soils.

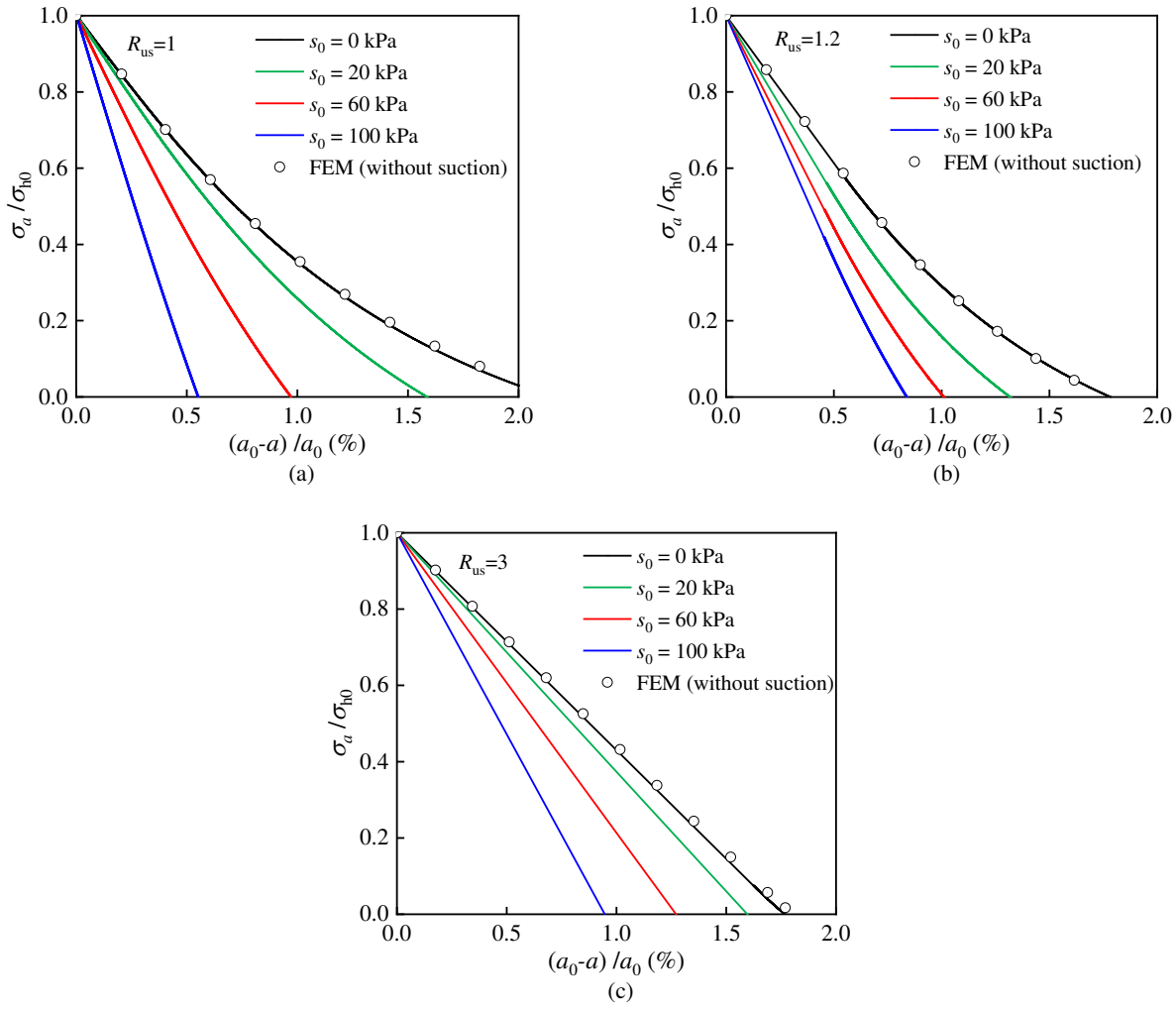

Figure 3 Influence of suction on GRCs: (a) R_{us}=1; (b) R_{us}=1.2; (c) R_{us}=3

To further explore the suction effect, Figure 4 plots the stress paths for a soil particle at $r=a$ in the normalised $p'-q$ plane. These paths end at the occasion when the internal support pressure decreases to zero (i.e. $\sigma_a=0$, marked by solid squares). Comparing the stress paths during cavity contraction in unsaturated and dry soils (Figure 4), two main features can be observed:

(a) The particle for unsaturated soils goes a much shorter stress path than that in dry soils. In fact, the effective radial stress at $r=a$ can be expressed as $\sigma_r'=\sigma_a+S_r s_0>0$ for unsaturated soils (see Eq.

(4)), while $\sigma_r' = \sigma_a = 0$ for soils without suction. Therefore, the suction effect on the effective stress is an important reason for the shorter stress paths in the $p'-q$ plane.

(b) After yielding occurs, unsaturated soils can bear a higher deviatoric stress at the same p' and R_{us}. This is because soil suction leads to the expansion of yield surfaces (see Eq. (7) and Figure 2). Accordingly, the suction effect on effective stresses and yield surfaces is also the reason for the variation of GRCs with soil suction.

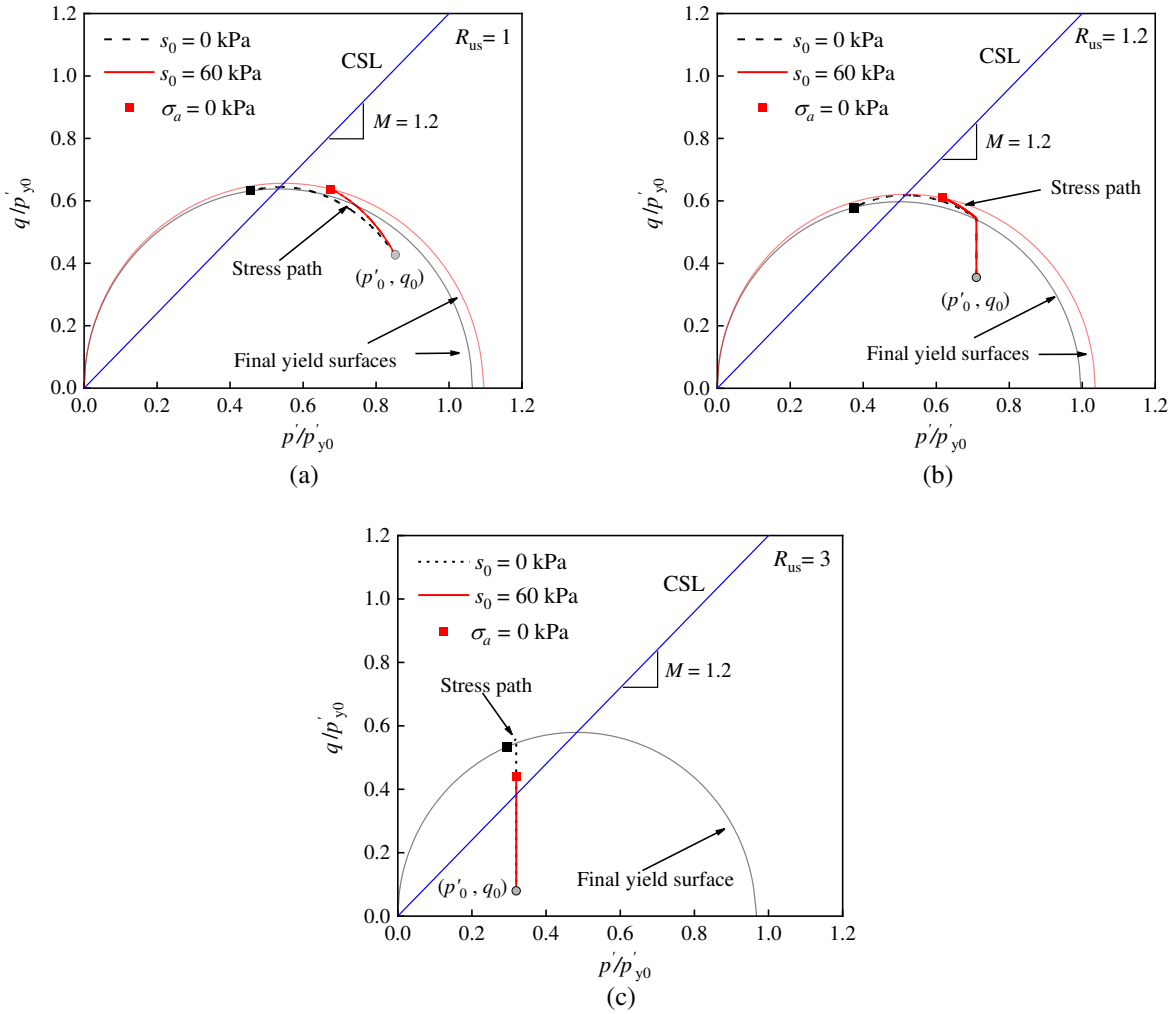

Figure 4 Stress paths for unsaturated and dry soils: (a) R_{us}=1; (b) R_{us}=1.2; (c) R_{us}=3

Figure 5 shows the distributions of effective radial, circumferential, and vertical stresses at the occasion of $\sigma_a = 0$. For unsaturated soils the effective radial stress at $r = a$ is positive instead of reducing to zero, which is consistent with $\sigma_r' = \sigma_a + S_r s_0 > 0$. When compared with the case without suction, the unloading-induced plastic zone becomes narrower for unsaturated ground, but the maximum circumferential effective

stress tends to be larger. Hence, the stress distribution results indicate that the effective stresses are not fully released due to the suction effect in unsaturated soils. In the long-time period when soils are wetted (i.e. suction decrease), stress redistribution may occur around tunnels and the unloading-induced plastic zone may expand further.

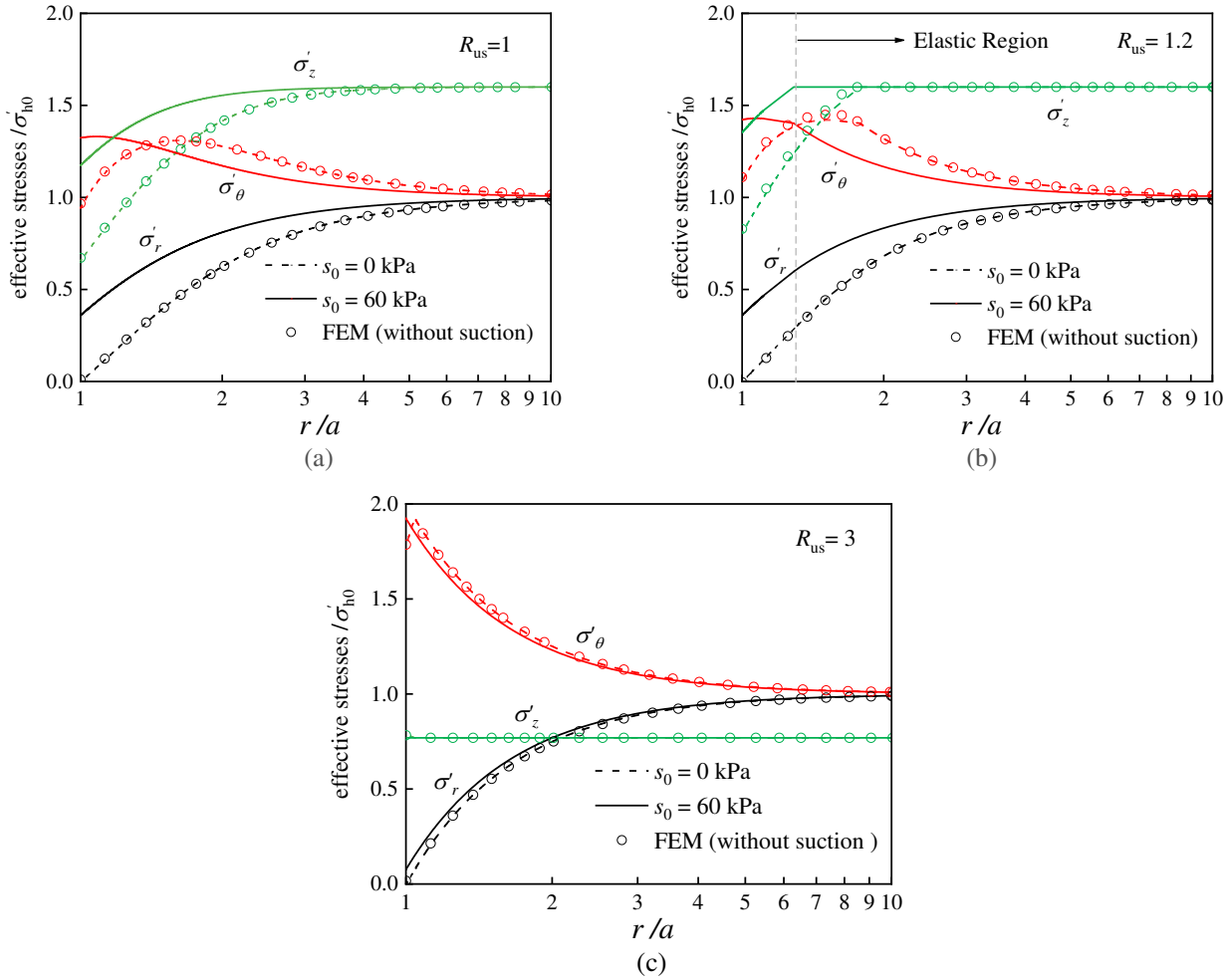

Figure 5 Stress distributions for unsaturated and dry soils: (a) R_{us} =1; (b) R_{us} =1.2; (c) R_{us} =3

Conclusions

An elastoplastic solution is developed for cavity contraction in unsaturated soils under constant suction conditions to investigate the influence of soil suction on GRCs. The equilibrium equation, constitutive equations for unsaturated soils, and continuity equation for the cavity contraction problem are transformed into a system of first-order ODEs by introducing a new auxiliary variable. After validating the solution accuracy, the effects of soil suction and overconsolidation ratio on GRCs, stress paths, and stress distributions are investigated. It is found that for a larger suction and overconsolidation ratio, the internal support pressure reduces faster with tunnel convergence. The soil particle for unsaturated soils goes a shorter stress path due to

the influence of suction on effective stresses and yield surfaces. Finally, stress distributions indicate that the effective stresses around unsaturated tunnels may not be fully released. The proposed solution can also be useful for wellbore drilling problems in unsaturated soils.

Acknowledgement

We would like to acknowledge the financial support from the National Natural Science Foundation of China (52108374), the "Taishan" Scholar Program of Shandong Province, China (tsqn201909016), the Shandong Provincial Natural Science Foundation (ZR202102250562), and the Key Basic Research Project of China (No.2022YFC3005604). The last author would also like to thank the financial support from the China Scholarship Council for his study at the University of Leeds.

Notation List

a, a_0	initial and current radius of cavity wall
b, c	material parameters for unsaturated soils
$\mathrm{D}(\bullet)$, $\mathrm{d}(\bullet)$	material time and spatial differentials of $(\bullet)$
E	Young's modulus
f	yield function
M	slope of critical state line
p_0', p'	initial and current effective mean stress
$p_{\mathrm{y}}'(0)$, $p_{\mathrm{y}}'(s)$	yield stresses for saturated and unsaturated soils
p_{y0}'	initial isotropic pre-consolidation stress
q, q_0, q_ρ	deviator stress, initial deviator stress, and deviator stress at the elastoplastic boundary
r_0, r	initial and current radial positions of a soil particle
R_{us}	overconsolidation ratio
s_0, s	initial and current suction
S_{r0}, S_{r}	initial and current degree of saturation
u	radial displacement of a soil particle
u_{a}, u_{w}	pore air and water pressures
v_0, v	initial and current specific volumes
$\varepsilon_r^{\mathrm{e}}$, $\varepsilon_\theta^{\mathrm{e}}$, $\varepsilon_z^{\mathrm{e}}$	elastic radial, circumferential and vertical strains
ε_r, ε_θ, ε_z	radial, circumferential and vertical strains

ε_v, $\varepsilon_v^{\mathrm{p}}$	total and plastic volumetric strains
κ	slope of loading–reloading line in $v-\ln p'$ plane
$\lambda(0)$, $\lambda(s)$	slopes of the normal compression lines for saturated and unsaturated soils
λ_{se}	slope of the $S_{\mathrm{r}}-v$ curve at constant suction
μ	Poisson's ratio of soil
ρ_0, ρ	initial and current radii of elastic-plastic boundary
η	stress ratio
σ_a	inner cavity pressure
σ_{h0}, σ_{v0}	in-plane and out-of-plane in-situ stress
σ'_{h0}, σ'_{v0}	in-plane and out-of-plane effective in-situ stress
σ_r, σ_θ, σ_z	total radial, circumferential, and vertical stresses
σ'_r, σ'_θ, σ'_z	effective radial, circumferential, and vertical stresses

References

Alonso, E. E., Gens, A. and Josa, A. (1990). "A constitutive model for partially saturated soils." Géotechnique **40**(3): 405-430.

Brown, E. T., Bray, J. W., Ladanyi, B. and Hoek, E. (1983). "Ground response curves for rock tunnels." Journal of Geotechnical Engineering **109**(1): 15-39.

Cai, W., Zhu, H., Liang, W., Wang, X., Su, C. and Wei, X. (2023). "A post-peak dilatancy model for soft rock and its application in deep tunnel excavation." Journal of Rock Mechanics and Geotechnical Engineering **15**(3): 683-701.

Carranza-Torres, C. (2003). "Dimensionless graphical representation of the exact elasto-plastic solution of a circular tunnel in a Mohr-Coulomb material subject to uniform far-field stresses." Rock Mechanics and Rock Engineering **36**(3): 237-253.

Chen, H., Feng, C. and Li, J. (2022). "An anisotropically elastoplastic solution to excavation responses of a circular opening considering three-dimensional strength." Acta Geotechnica **17**(9): 3995-4011.

Chen, H., Li, L. and Li, J. (2020). "Elastoplastic solutions for cylindrical cavity expansion in unsaturated soils." Computers and Geotechnics **123**: 103569.

Chen, S., Abousleiman, Y. and Muraleetharan, K. (2012). "Closed-form elastoplastic solution for the wellbore problem in strain hardening/softening rock formations." International Journal of Geomechanics **12**(4): 494-507.

Chen, S., Abousleiman, Y. and Muraleetharan, K. K. (2022). "Computational implementation of bounding surface model and its verification through cavity benchmark problems." International Journal for Numerical and Analytical Methods in Geomechanics **46**(3): 553-569.

Chen, S., Li, L. and Zhang, Z. (2020). Analysis of Cylindrical Cavity Expansion in Partially Saturated Soils. Geo-Congress 2020: Geo-Systems, Sustainability, Geoenvironmental Engineering, and Unsaturated Soil Mechanics, American Society of Civil Engineers Reston, VA.

Chen, S. L. and Abousleiman, Y. N. (2013). "Exact drained solution for cylindrical cavity expansion in

modified Cam Clay soil." Géotechnique **63**(6): 510-517.
Chen, S. L. and Abousleiman, Y. N. (2016). "Drained and undrained analyses of cylindrical cavity contractions by bounding surface plasticity." Canadian Geotechnical Journal **53**(9): 1398-1411.
Chen, S. L. and Abousleiman, Y. N. (2017). "Wellbore stability analysis using strain hardening and/or softening plasticity models." International Journal of Rock Mechanics and Mining Sciences **93**: 260-268.
Guan, K., Zhu, W., Yu, Q., Cui, L. and Song, F. (2022). "A plastic-damage approach to the excavation response of a circular opening in weak rock." Tunnelling and Underground Space Technology **126**: 104538.
Ma, Y., Zhu, H., Cai, W., Su, C. and Wei, X. (2023). "Analytical method for elastic-brittle-plastic analysis of a circular tunnel in a non-hydrostatic in-situ stress field considering the unified strength criterion." Applied Mathematical Modelling **121**: 780-799.
Mair, R. J. and Taylor, R. N. (1993). Prediction of clay behaviour around tunnels using plasticity solutions. Predictive Soil Mechanics: Proceedings of the Wroth Memorial Symposium, Oxford, UK, Thomas Telford.
Mo, P.-Q. and Yu, H.-S. (2017). "Undrained Cavity-Contraction Analysis for Prediction of Soil Behavior around Tunnels." International Journal of Geomechanics **17**(5): 04016121.
Park, K.-H., Tontavanich, B. and Lee, J.-G. (2008). "A simple procedure for ground response curve of circular tunnel in elastic-strain softening rock masses." Tunnelling and Underground Space Technology **23**(2): 151-159.
Su, D. (2021). "Drained solution for cylindrical cavity expansion in modified Cam Clay soil under constant vertical stress." Canadian Geotechnical Journal **58**(2): 176-189.
Sun, D. a., Sheng, D. and Sloan, S. W. (2007). "Elastoplastic modelling of hydraulic and stress–strain behaviour of unsaturated soils." Mechanics of Materials **39**(3): 212-221.
Sun, Z., Zhang, D., Fang, Q., Wang, J., Chu, Z. and Hou, Y. (2023). "Analysis of interaction between tunnel support system and surrounding rock for underwater mined tunnels considering the combined effect of blasting damage and seepage pressure." Tunnelling and Underground Space Technology **141**: 105314.
Vrakas, A. and Anagnostou, G. (2014). "A finite strain closed ‐ form solution for the elastoplastic ground response curve in tunnelling." International Journal for Numerical and Analytical Methods in Geomechanics **38**(11): 1131-1148.
Xu, C. and Xia, C. (2021). "A new large strain approach for predicting tunnel deformation in strain-softening rock mass based on the generalized Zhang-Zhu strength criterion." International Journal of Rock Mechanics and Mining Sciences **143**: 104786.
Yang, C., Chen, H. and Li, J. (2022). "Analysis of undrained cylindrical cavity contraction in anisotropic soils under constant total vertical stress condition." European Journal of Environmental and Civil Engineering: 1-18.
Yu, H.-S. (2000). Cavity expansion methods in geomechanics, Kluwer Academic Publishers, Dordrecht, The Netherlands.
Yu, H.-S. and Houlsby, G. T. (1991). "Finite cavity expansion in dilatant soils: loading analysis." Géotechnique **41**(2): 173-183.
Yu, H.-S. and Rowe, R. K. (1999). "Plasticity solutions for soil behaviour around contracting cavities and tunnels." International Journal for Numerical and Analytical Methods in Geomechanics **23**(12): 1245-1279.
Zareifard, M. R. (2020). "A new semi-numerical method for elastoplastic analysis of a circular tunnel excavated in a Hoek–Brown strain-softening rock mass considering the blast-induced damaged zone." Computers and Geotechnics **122**: 103476.

Zhao, Y., Wei, T., Wang, C. and Bi, J. (2023). "A New Close-Form Solution for Elastoplastic Seepage-Induced Stresses to Circular Tunnel with Considering Intermediate Principal Stress." Rock Mechanics and Rock Engineering **56**(9): 6545-6557.

Zhuang, P.-Z., Yang, H., Yue, H.-Y., Fuentes, R. and Yu, H.-S. (2022). "Plasticity solutions for ground deformation prediction of shallow tunnels in undrained clay." Tunnelling and Underground Space Technology **120**: 104277.

Zhuang, P.-Z., Yu, H.-S., Mooney, S. J. and Mo, P.-Q. (2020). "Loading and unloading of a thick-walled cylinder of critical-state soils: large strain analysis with applications." Acta Geotechnica **16**(1): 237-261.